Supporting information for: Ab Initio Electrochemistry: Exploring the Hydrogen Evolution Reaction on Carbon Nanotubes

Nico Holmberg, and Kari Laasonen*

COMP Centre of Excellence in Computational Nanoscience, Department of Chemistry, Aalto University, P.O. Box 16100, FI-00076 Aalto, Finland

E-mail: kari.laasonen@aalto.fi

*To whom correspondence should be addressed

Electrode Potential of Charged Nanotubes

In the main text, we showed that our model of the electrode-electrolyte interface was sufficiently accurate for determining a reliable estimate of the nanotube potential of zero charge. Here, we analyse how changing the nanotube surface charge affects the accuracy of the model for predicting electrode potentials and demonstrate that relative energies – in particular, grand canonical activation energies – are insensitive to any ambiguity in potential.

As opposed to charge neutral simulations, the electrode potential of a charged surface cannot directly be evaluated by referencing the Fermi level to the Volta potential (= vacuum potential) due to inclusion of the neutralizing background charge. Instead, we use a potential alignment term to reference the charged system Fermi level to the Volta potential of the charge neutral simulation, as demonstrated in Figure 1 of the main text. We chose to align the system potentials at the electrostatic potential minimum of the first solvation layer. An equally valid choice would be the potential maximum between the first and second solvation layers. The limited number of water molecules in our simulation system prevents using any other point as reference. Indeed, the close proximity of the vacuum interface causes the structure and hence the electrostatic potential of water to fluctuate at larger distances (measured from the nanotube tube axis), so that no well-defined reference point can be defined. Furthermore, the effects of the background charge are more profound in this region. Ideally, one could use enough water molecules that a true bulk water region would form and set the reference there, but at present this is computationally too demanding.

If we change the location of the potential alignment term to the maximum between the first and second solvation layers, the calculated, charged system electrode potentials are shifted by approximately $q \times 0.1$ V. While this seems like a large shift, it turns out that this shift cancels when grand canonical activation energies are constructed from the fitted parabolas to the data corrected energy vs electrode potential (see Figure 5 in the main text). For example, using the calculated minimum energy paths for the Volmer reaction on NCNT, the absolute difference between grand canonical activation energies computed with the different potential alignment definitions remains below 0.05 eV for the relevant potential region $U = -2$ V to $U = 0$ V, as illustrated in Figure S1.

As this error is well below the expected 0.1 eV accuracy for GGA level DFT, it can safely be neglected.

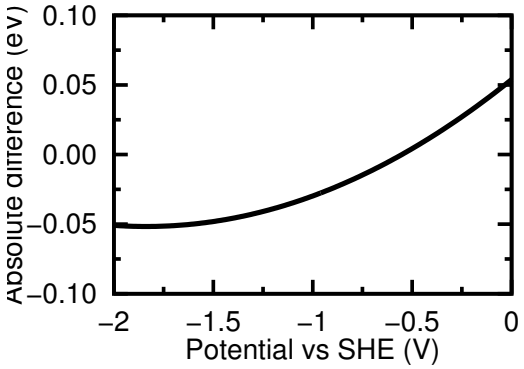

Figure S1. Absolute difference between Volmer reaction grand canonical activation energies calculated using different definitions for the potential alignment term.

While the previous analysis illustrates that the errors due to the ambiguous nature of the potential alignment term are not significant for valid alignment choices in the present system, it remains unclear how the error behaves as a function of system size if the number of water layers was increased to accommodate bulk water formation. At present, we are unable to address this matter since adding the sufficient water molecules is computationally too demanding, as noted previously. Nonetheless, seeing as our primary goal is to compare NCNT and CNT, this issue does not influence comparison since the same methodology has been consistently applied to both nanotubes and cancels out when comparing the electrodes. Moreover, we note that the potential (and naturally the electrode charge) dependent results presented herein and in the main text are fully consistent with the results obtained in charge neutral systems, which are devoid of any errors apart from inherent DFT errors. When combined with the fact that the results are fully reasonable from a purely qualitative viewpoint (barriers and reaction energies decrease when going towards more negative potential), this analysis demonstrates that the potential dependent results are at least qualitatively accurate. We are unfortunately unable to discuss the quantitative accuracy of our results in comparison to experimental values beyond what is already included in the main text (onset potential) due to lack of comparable data.

To estimate the effects of surface charging on electrode potential, we used select configurations

from the charge neutral system molecular dynamics simulation and computed the electrode potential with charges $q = -3$ to $q = +1$. While the true dynamics of a charged system wont exactly follow that of the neutral system, this scheme allows us to estimate how the electrode potential changes during NEB simulations because the majority of the water molecules will be frozen. As shown in Figure S2, electrode potential depends linearly on nanotube charge and charges $q = -3$ to $q = +1$ cover roughly a 2 V potential window.

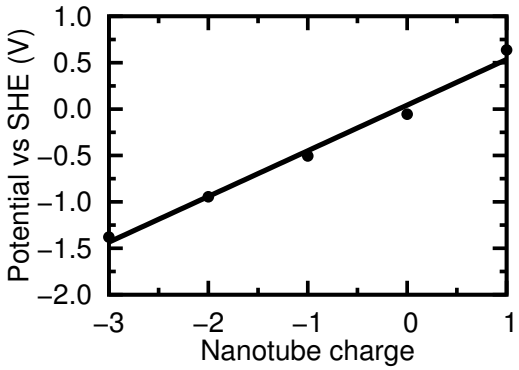

Figure S2. Electrode potential dependence on nanotube charge. The data points correspond to average values calculated at instantaneous atomic configurations of the neutral system molecular dynamics simulation. The configurations were chosen at 0.25 ps intervals between $1.0 - 4.5$ ps of the MD simulation. Fit coefficient of determination $R^2 = 0.989$.

Hydrogen Adsorption Calculations

To determine the most stable surface site for the electrochemical adsorption of a proton (the Volmer reaction) on NCNT, we calculated Gibbs energies of hydrogen adsorption ΔG_{ads} to sites near the nitrogen dopant in vacuum. The explored surface sites are labeled according to Figure S3. Employing the standard thermodynamic definition of Gibbs energy, ΔG_{ads} is given by

$$\Delta G_{ads} = \Delta E_{ads} + \Delta ZPE - T\Delta S_{ads} \tag{1}$$

where ΔE_{ads}, ΔZPE and ΔS_{ads} are the changes of energy, zero-point energy and entropy during adsorption, respectively, and T is temperature. As the reference state in calculating ΔG_{ads}, we choose molecular hydrogen H_2 at standard conditions ($p = 1$ bar, $T = 298$ K). Thus, the adsorption

energy ΔE_{ads} can be calculated from

$$\Delta E_{ads} = E_{\mathrm{NCNT+H}} - E_{\mathrm{NCNT}} - \frac{1}{2} E_{\mathrm{H_2}} \tag{2}$$

where E_{NCNT}, $E_{\mathrm{H_2}}$ and $E_{\mathrm{NCNT+H}}$ are the absolute energies of the clean NCNT, gas-phase hydrogen and the NCNT with an adsorbed hydrogen atom, respectively. These energies are obtained by performing geometry optimizations on the corresponding states. In geometry optimization, we use a maximum force converge criterion of 0.023 eV/Å.

Following Nørskov et al.,[1] we use vibrational analysis to determine the changes in zero-point energy ΔZPE and entropy ΔS_{ads} upon adsorption. Specifically, the normal mode of adsorbed hydrogen is evaluated at each surface site. Because the vibrational entropy of the adsorbed atom is well below 1 meV, the adsorption entropy is directly given by the standard entropy of molecular hydrogen $\Delta S_{ads} = -\frac{1}{2} S^0_{H_2}$. For gas-phase hydrogen at standard conditions, we use tabulated thermodynamic data: $-\frac{1}{2} T S^0_{H_2} = 0.20$ eV and $ZPE_{\mathrm{H_2}} = 0.55$ eV.[2]

Calculated Gibbs energies of hydrogen adsorption ΔG_{ads} as well as the related adsorption energies ΔE_{ads} and zero-point energy changes ΔZPE are shown in Table S1 for adsorption onto pristine and nitrogen doped CNTs. For NCNT, data for the adsorption of a second hydrogen atom is also included.

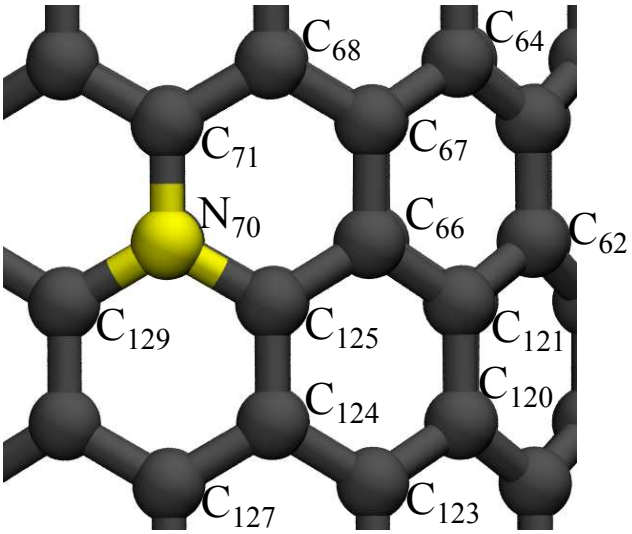

Figure S3. Labeling of atoms near the nitrogen dopant. Carbon atoms are in gray, nitrogen is in yellow.

Structural Data for the Volmer Reaction

Table S1. Calculated Gibbs energies of hydrogen adsorption ΔG_{ads} (in eV) to different surface sites on the nitrogen doped and pristine carbon nanotubes. Also shown are the calculated adsorption energies ΔE_{ads} and zero-point energy changes ΔZPE that are used to determine ΔG_{ads}. In the right column, corresponding energies for the adsorption of a second hydrogen atom onto NCNT with site C_{125} already occupied.

1st H-atom				2nd H-atom			
Site	ΔE_{ads}	ΔZPE	ΔG_{ads}	Site	ΔE_{ads}	ΔZPE	ΔG_{ads}
C_{66}	0.50	0.14	0.85	C_{66}	0.40	0.10	0.71
C_{68}	0.42	0.10	0.72	C_{68}	0.66	0.17	1.03
N_{70}	1.24	0.16	1.61	N_{70}	1.59	0.23	2.03
C_{71}	0.02	0.11	0.33	C_{71}	0.52	0.17	0.89
C_{124}	0.52	0.14	0.87	C_{124}	0.00	0.18	0.39
C_{125}	−0.06	0.11	0.25	C_{129}	0.54	0.20	0.94
C_{129}	−0.06	0.15	0.29				
CNT	0.85	0.09	1.15				

Table S2. Structures of the Volmer reaction initial (IS), transition (TS) and final states (FS) on NCNT at different electrode charges q. Distances d are given in units of Å. H_1 denotes the reacting proton, $*$ is the active surface site, O_1 is the oxygen initially bonded to H_1, H_2 is the most acidic proton of the Zundel cation, O_2 is the second oxygen atom of the Zundel cation.

	$q=0$			$q=-2$			$q=-3$		
Distance	IS	TS	FS	IS	TS	FS	IS	TS	FS
d_{H_1-*}	2.01	1.39	1.15	1.96	1.50	1.14	1.95	1.59	1.13
$d_{H_1-O_1}$	0.99	1.26	1.66	1.00	1.18	1.63	1.00	1.13	1.67
$d_{O_1-H_2}$	1.23	1.05	1.00	1.19	1.06	1.00	1.19	1.07	1.00
$d_{H_2-O_2}$	1.21	1.51	1.67	1.25	1.48	1.64	1.26	1.44	1.65

Table S3. Structures of the Volmer reaction initial (IS), transition (TS) and final states (FS) on CNT at different electrode charges q. The labels of Table S2 apply to this table.

	$q=0$			$q=-2$			$q=-3$		
Distance	IS	TS	FS	IS	TS	FS	IS	TS	FS
d_{H_1-*}	2.13	1.34	1.17	1.98	1.49	1.12	1.91	1.68	1.10
$d_{H_1-O_1}$	0.99	1.38	1.71	1.01	1.25	2.08	1.02	1.36	2.25
$d_{O_1-H_2}$	1.23	1.03	1.00	1.16	1.04	0.99	1.13	1.08	0.99
$d_{H_2-O_2}$	1.21	1.61	1.73	1.29	1.53	1.82	1.33	1.45	1.84

Comparison of Grand Canonical and Constant Charge Activation Energies

In the main text, it was explained that an extrapolation scheme was employed to calculate grand canonical activation energies on a wider potential scale. The effects of this extrapolation scheme are illustrated in Figure S4. For comparison, the figure also includes the potential dependence of the constant charge (canonical) activation energies that are obtained by fitting a linear equation to the data activation energy vs average electrode potential. All in all, there is no substantial difference in the grand canonical curves. If the extrapolation method is neglected, activation energies are only affected at the extremes of the studied potential range. However, in the case of the Volmer reaction, this leads to an unphysically low barrier (below 0 eV) at $U = -2$ V. Nevertheless, these differences are so minor that both methods essentially provide analogous information of the reactions. By contrast, the canonical activation energies depend too strongly on potential and deviate from the grand canonical curves. Indeed, this the primary reason why constant potential activation energies are necessary in studying electrochemical reactions.

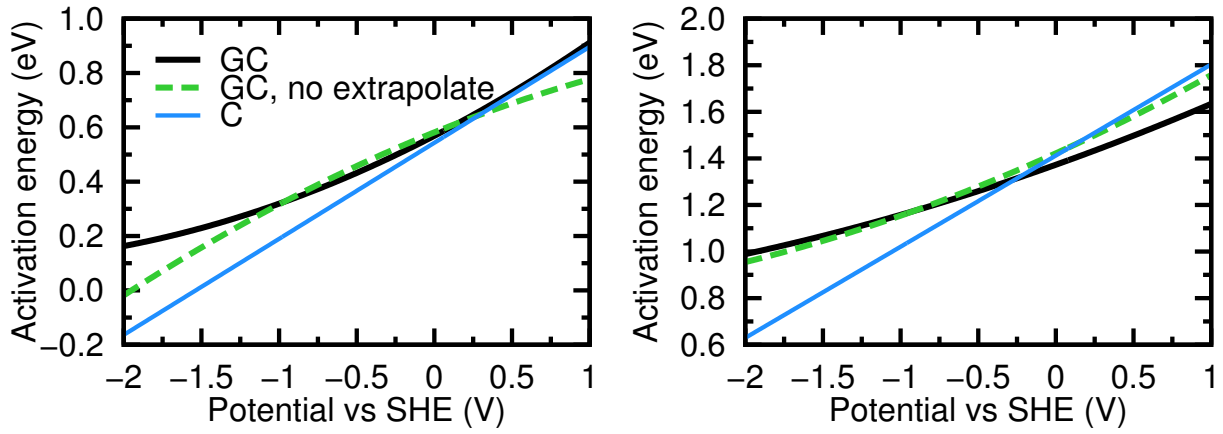

Figure S4. Comparison of Volmer (left) and Heyrovsky (right) reaction activation energies on NCNT and their dependence on electrode potential calculated with different methods. GC denotes grand canonical activation energies, while C denotes canonical activation energies. Grand canonical barriers are calculated with (same as main text Figures 5 and 8) and without the extrapolation method, which was detailed in the main text.

Second Volmer Reaction

The Volmer reaction of a second proton on NCNT was investigated using the same methodology that was employed for the first reaction, which has been detailed in the main text. As the active site in this reaction, we use surface atom C_{66} that is directly next to the first active site C_{125}. The calculated minimum energy paths at nanotube charges $q = 0, -1, -2$ and the constructed potential dependent grand canonical activation energies are shown in Figure S5. Compared to the first reaction (Figures. 4 and 5 in the main text), a 0.15 eV decrease in activation energies is observed. This clearly indicates that hydrogen atoms bound to the nanotube surface increase the reactivity of neighboring sites towards the Volmer reaction.

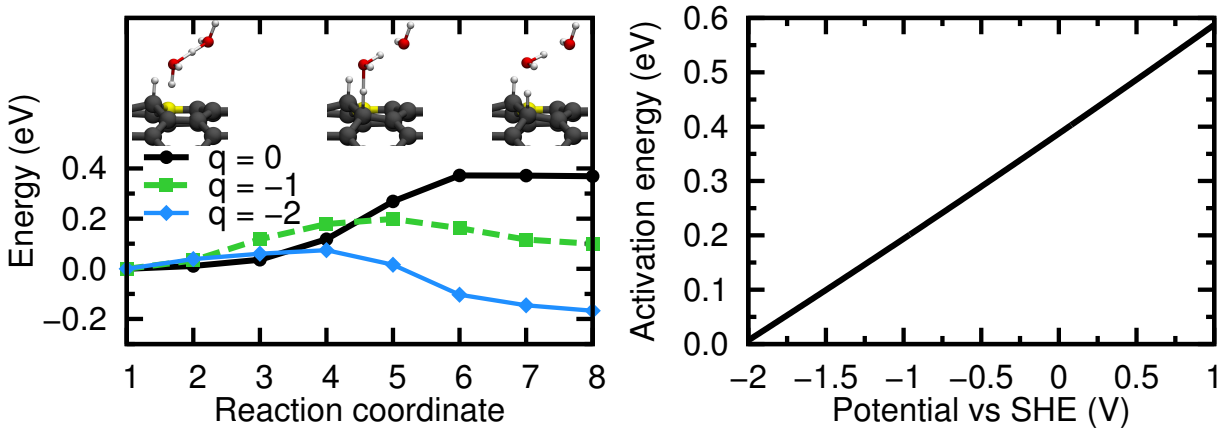

Figure S5. Calculated minimum energy paths for the second Volmer reaction on NCNT at different surface charges q (left). Electrode potential dependence of the reaction grand canonical activation energy (right).

Structural Data for the Heyrovsky Reaction

Table S4. Structures of the Heyrovsky reaction initial (IS), transition (TS) and final states (FS) on NCNT at different electrode charges q. Distances d are given in units of Å. H^* denotes the reacting surface hydrogen, $*$ is the active surface site, H_1 is reacting proton, O_1 is the oxygen initially bonded to H_1, H_2 is the most acidic proton of the Zundel cation, O_2 is the second oxygen atom of the Zundel cation.

	$q=0$			$q=-1$			$q=-2$		
Distance	IS	TS	FS	IS	TS	FS	IS	TS	FS
d_{H^*-*}	1.11	1.55	2.73	1.11	1.56	2.73	1.11	1.50	2.74
$d_{H^*-H_1}$	1.92	0.92	0.73	1.91	0.91	0.73	1.93	0.94	0.73
$d_{H_1-O_1}$	0.98	1.39	2.56	0.99	1.39	2.55	0.99	1.35	2.55
$d_{O_1-H_2}$	1.36	1.04	0.99	1.35	1.04	0.99	1.34	1.05	0.99
$d_{H_2-O_2}$	1.11	1.50	1.80	1.12	1.50	1.80	1.12	1.47	1.81

Table S5. Structures of the Heyrovsky reaction initial (IS), transition (TS) and final states (FS) on CNT at different electrode charges q. The labels of Table S4 apply to this table.

	$q=0$			$q=-1$			$q=-2$		
Distance	IS	TS	FS	IS	TS	FS	IS	TS	FS
d_{H^*-*}	1.11	1.48	2.75	1.11	1.43	2.76	1.12	1.43	2.76
$d_{H^*-H_1}$	1.86	0.94	0.73	1.87	0.96	0.73	1.87	0.96	0.73
$d_{H_1-O_1}$	0.98	1.35	2.61	0.99	1.32	2.62	0.99	1.32	2.62
$d_{O_1-H_2}$	1.36	1.05	0.99	1.35	1.06	0.99	1.35	1.06	0.99
$d_{H_2-O_2}$	1.11	1.47	1.80	1.12	1.45	1.81	1.12	1.45	1.81

Grand Canonical Reaction Energies

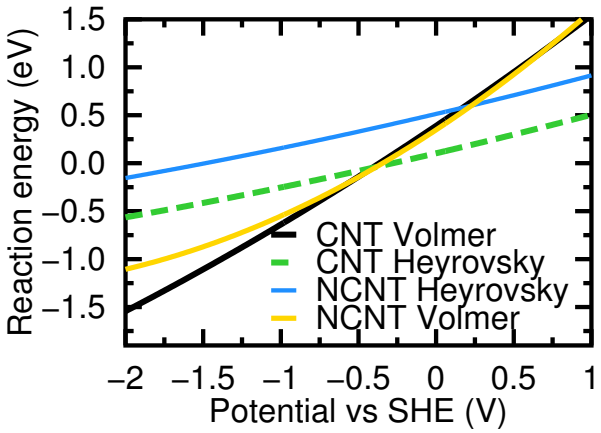

Figure S6. Grand canonical reaction energies of the Volmer and Heyrovsky reactions on NCNT and CNT as a function of electrode potential.

Potential Dependent Energy Diagrams for the Volmer-Heyrovsky Reaction

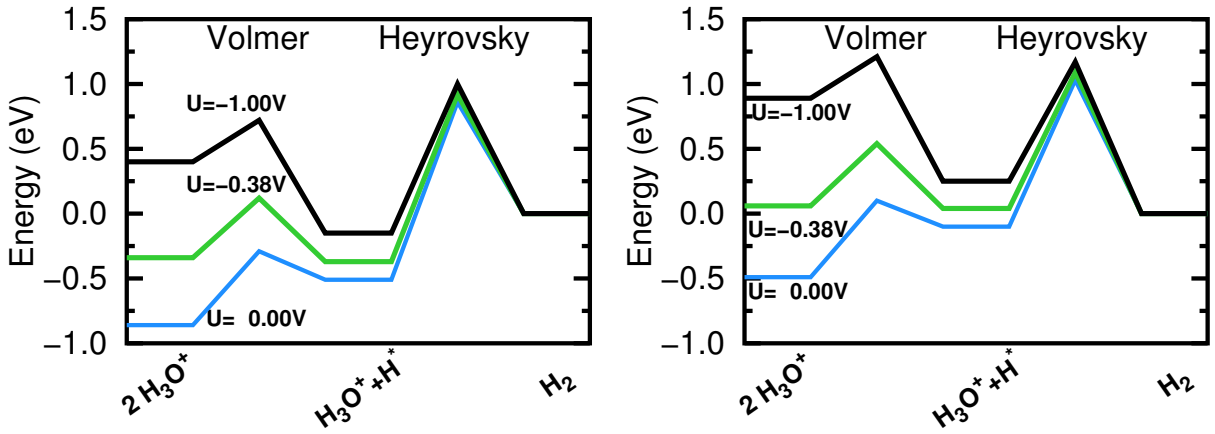

Figure S7. Energy diagrams for HER proceeding through the Volmer-Heyrovsky mechanism on NCNT (left) and CNT (right) at selected electrode potentials.

Calculation of Standard Free Energies, Coverage and Onset Potential

Using the Volmer and Heyrovsky reaction equations that are defined in the main text, the standard reaction free energies of these steps can be written as

$$\Delta G^{\mathrm{i}}(U) = \Delta\Omega^{\mathrm{i}}(U) + T\Delta S^{\mathrm{i}} + \Delta ZPE^{\mathrm{i}} \tag{3}$$

where $i = \{\mathrm{Volmer}, \mathrm{Heyrovsky}\}$, $\Delta\Omega^{\mathrm{i}}(U)$ is the potential dependent reaction energy from Figure S6 and

$$\Delta ZPE^{\mathrm{Volmer}} = ZPE_{\mathrm{H^*}} + ZPE_{\mathrm{H_2O}} - ZPE_{\mathrm{H_3O^+}} \tag{4}$$

$$\Delta S^{\mathrm{Volmer}} = S_{\mathrm{H_2O}} - S_{\mathrm{H_3O^+}} \tag{5}$$

$$\Delta ZPE^{\mathrm{Heyrovsky}} = ZPE_{\mathrm{H_2}} + ZPE_{\mathrm{H_2O}} - ZPE_{\mathrm{H^*}} - ZPE_{\mathrm{H_3O^+}} \tag{6}$$

$$\Delta S^{\mathrm{Heyrovsky}} = S_{\mathrm{H_2}} + S_{\mathrm{H_2O}} - S_{\mathrm{H_3O^+}} \tag{7}$$

For H_2O and H_3O^+, we use tabulated ideal gas values at standard conditions for the entropy terms while high level ab initio data are used for the zero-point energy terms, as summarized in Table S6. For H_2, we employ the same thermodynamic data that was used to compute adsorption free energies. The ZPE of H^* was determined using vibrational analysis and was separately evaluated for NCNT and CNT, see Table S6.

To calculate activation free energies, we only consider the effects of zero-point energy.[3] The expressions are otherwise analogous to Equation 3 and the ZPE terms are given by

$$\Delta ZPE_a^{\text{Volmer}} = ZPE_{TS}^{\text{Volmer}} + ZPE_{\text{H}_2\text{O}} - ZPE_{\text{H}_3\text{O}^+} \tag{8}$$

$$\Delta ZPE_a^{\text{Heyrovsky}} = ZPE_{TS}^{\text{Heyrovsky}} + ZPE_{\text{H}_2\text{O}} - ZPE_{\text{H}^*} - ZPE_{\text{H}_3\text{O}^+} \tag{9}$$

$$\tag{10}$$

The reaction transition state ZPEs are evaluated using vibrational analysis by considering frequencies associated with the protons that are reduced in the reactions, as illustrated in Table S6.

Table S6. Zero-point energies (ZPE, in eV) and entropies at 298 K (TS, in eV) used in calculating activation and reaction free energies.

Species/State	*ZPE*	*TS*
H_2	0.546[2]	0.408[2]
H_2O	0.575[4]	0.587[5]
H_3O^+	0.924[6]	0.598[5]
H^*_{CNT}	0.378	-
H^*_{NCNT}	0.405	-
Volmer TS_{CNT}	0.390	-
Volmer TS_{NCNT}	0.432	-
Heyrovsky TS_{CNT}	0.421	-
Heyrovsky TS_{NCNT}	0.457	-

As a first approximation, the nanotube hydrogen coverage can be evaluated as a function of potential using the Volmer reaction free energy $\Delta G^{\text{Volmer}}(U)$ from Figure S6 and a non-interacting Langmuir model

$$\theta(U) = \frac{K}{1+K}; \quad K = \exp\left(-\frac{\Delta G^{\text{Volmer}}(U)}{k_B T}\right) \tag{11}$$

For pristine CNT, this model yields the coverage-potential dependence shown in Figure S9. To estimate the coverage on NCNT, we assume that the effects of nitrogen doping are contained to nearest neighbor carbons, so that the remaining sites behave as they would on pristine CNT. The total coverage is then given by the sum of coverages on these two site types. Additionally, it is assumed that direct reactions to the nitrogen atom are impossible and that all the carbon atoms next

to the dopant are equivalent. Due to the near identical Volmer reaction free energies on NCNT and CNT, see Figure S6, the coverages of both sites follow the same potential dependence and reach maximum coverage at $U = -0.5$ V. Of course, the total maximum coverage on NCNT is slightly lower than on pristine CNT due to the inactive nitrogen sites.

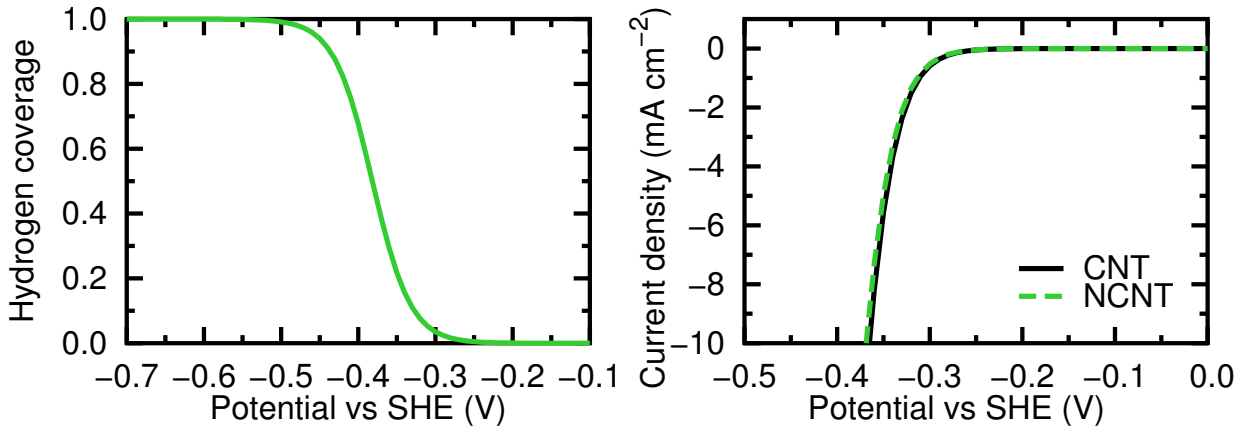

Figure S8. Surface hydrogen coverage on pristine CNT as a function of electrode potential calculated using a Langmuir model (left). Estimation of the computational onset potential on CNT and NCNT (right) using the kinetic model that is presented in the main text.

Volmer-Heyrovsky Reaction Energy Dependence on Surface Hydrogen Coverage

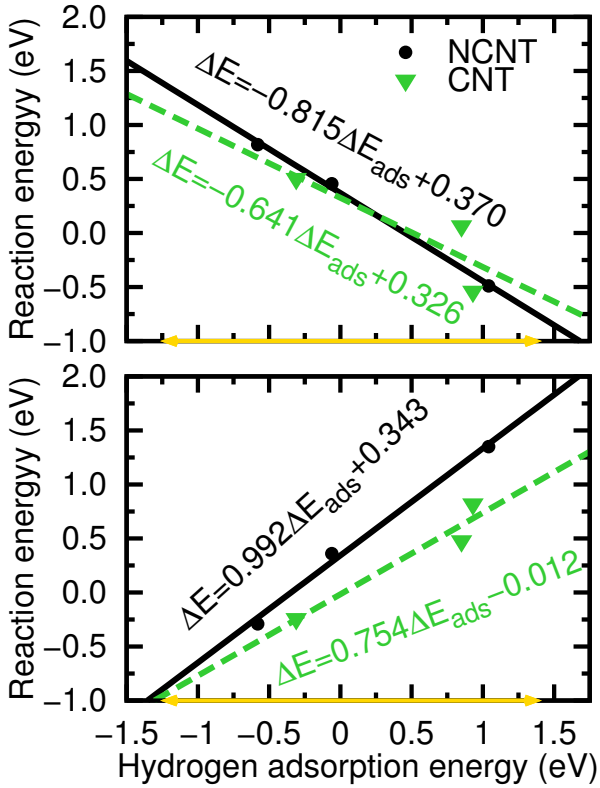

Figure S9. Calculated Heyrovsky (top) and Volmer (bottom) reaction energies on NCNT and CNT as a function of hydrogen adsorption energy, measured for adsorption onto the active surface site. Different activation energies correspond to a distinct distribution of adsorbed hydrogen atoms near the active site (points). The lines are linear fits to the individual data points with equations indicated. The range of observed adsorption energies on NCNT is shown by the yellow arrow. $R^2 = 0.998, 0.719, 0.992, 0.932$ (top-to-bottom order)

Adsorption Energy Dependence on Surface Hydrogen Coverage

Table S7. Calculated hydrogen adsorption energies ΔE_{ads} (in eV) onto site C_{125} on the nitrogen doped carbon nanotube at different surface hydrogen coverages. Sites already occupied by hydrogen atoms near the active site are indicated in the first column. Change in adsorption energy $\Delta(\Delta E_{ads})$ relative to the value on the clean surface (first row) is shown in the last column.

Occupied sites	ΔE_{ads}	$\Delta(\Delta E_{ads})$
–	−0.06	–
C_{66}	−0.16	−0.10
C_{67}	0.65	0.72
C_{68}	0.18	0.24
C_{71}	0.44	0.51
C_{121}	0.46	0.53
C_{124}	−0.58	−0.52
C_{127}	0.60	0.67
C_{129}	0.55	0.61
C_{66}, C_{67}	−0.49	−0.42
C_{66}, C_{124}	−1.22	−1.16
C_{67}, C_{121}	1.37	1.43
C_{67}, C_{127}	1.04	1.10
C_{71}, C_{129}	0.59	0.65
C_{121}, C_{127}	0.82	0.88
C_{67}, C_{121}, C_{127}	0.86	0.92
$C_{67}, C_{121}, C_{123}, C_{127}$	1.23	1.29
$C_{64}, C_{66}, C_{68}, C_{123}, C_{127}$	0.69	0.75
$C_{67}, C_{121}, C_{123}, C_{127}, C_{129}$	1.11	1.17
$C_{67}, C_{71}, C_{121}, C_{123}, C_{127}, C_{129}$	1.32	1.38
$C_{62}, C_{64}, C_{66}, C_{68}, C_{71}, C_{120}, C_{123}, C_{127}, C_{129}$	0.78	0.84

Table S8. Same as Table S7, but for adsorption onto site C_{125} on the pristine carbon nanotube. Sites on the pristine CNT are also labeled according to Figure S3 but with site N_{70} replaced by C_{70}.

Occupied sites	ΔE_{ads}	$\Delta(\Delta E_{ads})$
–	0.85	–
C_{67}	0.95	0.10
C_{124}	−0.31	−1.15
C_{127}	0.95	0.10
C_{66}, C_{124}	−0.92	−1.77
C_{67}, C_{121}	1.06	0.21
C_{67}, C_{127}	0.93	0.08
C_{66}, C_{67}, C_{127}	0.23	−0.62
C_{67}, C_{121}, C_{127}	1.45	0.61
$C_{67}, C_{121}, C_{123}, C_{127}$	1.14	0.29

References

(1) Nørskov, J. K.; Bligaard, T.; Logadottir, A.; Kitchin, J. R.; Chen, J. G.; Pandelov, S.; Stimming, U. Trends in the Exchange Current for Hydrogen Evolution. *J. Electrochem. Soc.* **2005**, *152*, 23–26.

(2) Atkins, P.; de Paula, J. *Atkins' Physical Chemistry*, 7th ed.; Oxford University Press, 2002; pp 1080–1097.

(3) Rossmeisl, J.; Skúlason, E.; Björketun, M. E.; Tripkovic, V.; Nørskov, J. K. Modeling the Electrified Solid–Liquid Interface. *Chem. Phys. Lett.* **2008**, *466*, 68–71.

(4) Mátyus, E.; Czakó, G.; Sutcliffe, B. T.; Császár, A. G. Vibrational Energy Levels with Arbitrary Potentials Using the Eckart-Watson Hamiltonians and the Discrete Variable Representation. *J. Chem. Phys.* **2007**, *127*, 084102.

(5) Chase Jr., M. *J. Phys. Chem. Ref. Data*; NIST Standard Reference Data, Monograph 9, 1998; pp 1–1963.

(6) Rajamäki, T.; Miani, A.; Halonen, L. Six-dimensional Ab Initio Potential Energy Surfaces for H_3O^+ and NH_3: Approaching the Subwave Number Accuracy for the Inversion Splittings. *J. Chem. Phys.* **2003**, *118*, 10929–10938.